

Identifying objects in a 2D-space utilizing a novel combination of a re-radiation based method and of a difference-image-method

Andreas Sebastian SCHMELT¹; Torben MARHENKE²; Jens TWIEFEL³

^{1,2,3} Institute of Dynamic and Vibration Research; Leibniz University Hannover, Germany

ABSTRACT

To identify objects in a 2D space the feasibility of a novel attempt is investigated in this study. The acoustic fields are simulated utilizing the 2D finite difference K-Wave toolbox in MATLAB. The generated acoustic field is recorded at defined positions that can be understood as receiver positions. From these data, the acoustic field is recalculated using the 2D-re-radiation-method. An object-free acoustic field serves as reference. The acoustic field (at the receiver) considering the object is determined. The full acoustic field is recalculated from the secondly recorded data. Using a difference-image-method, the calculated acoustic fields are processed and the position, size and geometric shape is identified from the remaining diffraction pattern. Different objects and object positions are studied. Furthermore, the influence of different excitation signals of the transducer for the identification are investigated.

Keywords: Re-radiation, Air coupled ultrasound, Object identification

1. INTRODUCTION

For non-destructive testing (NDT), ultrasonic methods in a liquid medium are often used to get matching impedance characteristics. Some Testing objects can't be placed in liquid media. Air-coupled ultrasound (ACU) is applied for these type of objects as an alternative method ACU is commonly used to identify objects or inhomogeneities of materials in several situations, e.g. for the identification of cans in a product line [6] or structures in a wood plate [7].

In this study, 2D simulations of airborne sound fields are performed. The MATLAB toolbox k-wave is used for the simulation. The sound propagation in the 2D space is determined by ultrasonic excitation at frequencies up to 50 kHz. Different objects are placed in this space. The simulated sound pressure signal is recorded and stored via defined points, which can be understood as microphone positions of a B-scan.

Usually pulsed signals are used for ACU-measurements [2, 4, 6, 7], but the control electronics for this type of signal are usually more complex and the ultrasonic transducers have a different design than for harmonic signals. Therefore, we study here the comparability of the used methods with a pulsed signal to a multiharmonic signal. The multiharmonic signal is modeled by selecting of the correct excitation frequencies to generate a beat signal. When setting certain sections to zero, there will be got a quasi-pulsed signal in the recorded time signal. This results in almost identical results like those with the pulsed signal. This offers the possibility to use simpler control electronics later, as well as ultrasonic transmitters where resonant excitation and low attenuation are desired.

An innovative method to reconstruct the airborne sound fields, from recorded sound pressure signals, is the re-radiation method [1, 2, 8, 9]. The propagation path of the sound waves can be reconstructed from the recorded data by calculating backwards in time (backward propagation) or forwards in time (forward propagation). This method is used here to reconstruct the sound pressure field to represent experimental conditions. Because in B-scan or A-scan experiments, one does not know how the sound field looked like, only the recorded time data at the microphone positions are known. Due to its mathematical origin, the re-radiation method only reconstructs sound paths; it is not clear whether objects were on the way. Only the diffraction of the sound waves can be

¹ schmelt@ids.uni-hannover.de

² marhenke@ids.uni-hannover.de

³ twiefel@ids.uni-hannover.de

reconstructed. One way to identify objects is to look for the places where the sound pressure drops, because the sound waves first have to diffract around the object, creating a sound shadow behind the object. Due to the impedance jump from air to the most of other stuffs, e.g. like plastic, wood or steel, the most acoustic energy will be reflected from the solid surface and not transmitted. In this way, delaminations in wooden panels are detected in [9]. The authors from [2] were also able to estimate the position of plastic beads in this way.

Difference-image-methods are often used to identify moving objects in videos out of many frames. The challenge is to find a good threshold for the identification. In [3] the authors present techniques to identify motions in a set of frames and shadow detection algorithms using difference-image methods. They show the possibility of the identification depends on the correct threshold estimation for the evaluation of the difference images.

With the approach proposed here, the object-free reconstructed airborne sound field is used as a reference image and analyzed with the object-afflicted reconstructed airborne sound fields using a difference-image method. This makes it possible to use the entire reconstructed sound field and not only the sound pressure drops at the object position from the re-radiation method for object identification. From the difference images using suitable threshold values, border images are generated from which not only the size and position of the object can be determined, but also its geometric shape. For this, three fundamental geometric shapes made of PMMA are used. Furthermore, peak border images of the mean absolute deviation are determined, on the basis of which it is also possible to determine the position, shape and size of the objects. The new approach is to use difference-image methods of a reconstructed airborne sound field to identify object size, position and geometric shape. This could improve e.g. the product inspection during the process on a production line.

2. Methods

2.1 Simulation setup

For the simulation of the acoustic fields the 2D finite difference toolbox for MATLAB named K-Wave, is used. K-Wave use for the calculation a pseudospectral method in the k-space. The two advantages rather than other finite difference or finite element methods are first the efficiently amplitude calculation of the Fourier components using the fast Fourier transform and that the basic functions are sinusoidal so that theoretically only two grid points per wavelength are needed opposing to other methods which need six or ten grid points [5]. In Figure 1 on the left side the two excitation signals for the whole simulation time of 1.5 ms are depicted. At first is a sine pulse with a frequency of 50 kHz and ten oscillations at a maximum amplitude of 0.2 m/s. The transient response and decay behaviour is modelled with an exponential function and a damping coefficient of $\delta = -50000$ 1/s. The second is a multi-harmonic sine signal. This signal consists of two sine signals with frequencies of 48 kHz and 50 kHz each of them has an amplitude of 0.1 m/s. Thus, the resulting beat signal has an amplitude of 0.2 m/s and a beat frequency of 2 kHz. The transient response is the same as for the first excitation signal. The simulated airborne sound field (see Figure 1, right) is about 0.24 m x 0.33 m with a grid resolution of $dx = dy = 1.65e-4$ m which is less than $\lambda/40$. At all boundaries 20 elements are configured for as perfectly matched layers (PML), which are not depicted in the diagrams. The PML's has an anisotropic absorption of 2 Np/s. The surrounding medium is air with a sound velocity of $c = 343$ m/s and a density of $\rho = 1.24$ kg/m³. The media are modelled as sound absorbing media following the frequency power law:

$$\alpha = \alpha_0 \omega^h . \quad (1)$$

The air has a power law prefactor of $\alpha_0 = 0.01$ (rad/s)^{-h} Np/m. With the exponent for the frequency power law $h = 2$ for the whole simulated airborne sound field. In this study, objects in the far field are investigated. The transducer is modelled as a velocity source in y direction. At the receiver positions the sound pressure is recorded. The objects have material properties of PMMA with a density of $\rho_{obj} = 1190$ kg/m³, a sound velocity of $c_{obj} = 2540$ m/s and a frequency power law coefficients of $\alpha_{0,obj} = 1$ (rad/s)^{-h} Np/m. In the simulation only longitudinal waves are considered, no shear waves.

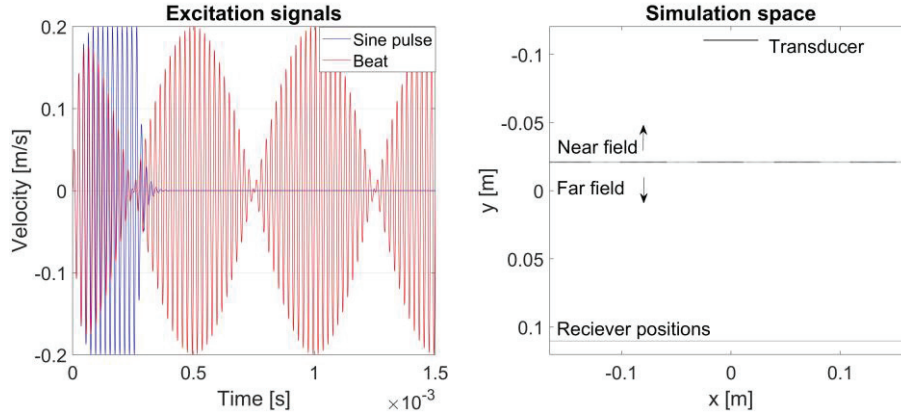


Figure 1 – The excitations signals (left) and the simulation space (right)

2.2 Re-radiation

With the re-radiation method, it is possible to calculate the propagation path of sound waves backwards or forwards in time from a single plane measurement. For each calculated plane on the path of the sound waves, the amplitudes can be depicted. This gives interpretable images of the maximum sound pressure fields. Using the Rayleigh integral for an arbitrary-pulsed scalar field in a 3D space is the fundament for the re-radiation method, which is used here. The derivation of the re-radiation equation follows [1] and [2]. The distance from the receiver positions to the propagated point is:

$$R = \sqrt{(x - x')^2 + y^2 + (z - z')^2}. \quad (2)$$

With the wave number k , the imaginary unit i and the propagation exponent V , with $V= 1$ for forward propagation or $V= -1$ for backward propagation, the free space Green's function G , which is an important part of the re-radiation method, is:

$$G = -\frac{e^{VikR}}{4\pi R}. \quad (3)$$

The arbitrary-pulsed scalar field becomes the following form:

$$p(x, y, z, \omega) = 2 \int_S p(x', 0, z', \omega) \frac{\partial G}{\partial y} dx' dz'. \quad (4)$$

The derivation of the Green's function with $V= -1$ (because only the backward propagation is of interest in this work) is:

$$\frac{\partial G}{\partial y} = \frac{e^{-ikR}}{4\pi R} \left(\frac{1}{R} + ik \right) \frac{y}{R}. \quad (5)$$

Inhomogeneous waves vanish for $R \gg \lambda/(2\pi)$, so the term $1/R$ can be neglected. For large distances from the transducer surface the term $y/R \cong 1$. This simplification increases the calculation speed significantly. With a finite measurement plane there is a pixel size h_p and with the simplified derivation of the Green's function G_s the pressure field can be implemented as:

$$p(x, y, z, \omega) \cong 2 h_p^2 p(x', 0, z', \omega) * G_s(x - x', y, z - z'). \quad (6)$$

Here means * the convolution of the pressure at the receiver positions with the derivative Green's function. The convolution can be interpreted as the summation of all proportion measuring points to each single calculated point of propagation plane. For the 2D pressure field the case of a line excitation a homogenous pressure field in z -direction is assumed. To convert equation 5, accordingly the simplified Green's function must be integrated over the z -direction:

$$G_s(x - x', y) = \int_{-\infty}^{\infty} G_s(x - x', y, z - z') dz = -\frac{i k y}{4 \sqrt{(x - x')^2 + y^2}} H_1^2 \left(k \sqrt{(x - x')^2 + y^2} \right). \quad (7)$$

Here is H_1^2 the tabulated Hankel function of the first order and second kind. So, the 2D pressure field can be calculated by:

$$p(x, y, \omega) \cong 2 h_p^2 p(x', 0, \omega) * G_s(x - x', y) \quad (8)$$

The free space the back propagated pressure field of the two signals is depicted in figure 2. A typical behaviour of a piston transducer is depicted for the sine pulse and for the beat signal. The pressure field is normalized to the maximum pressure which was recorded at all receivers (see figure 1, right) over the time in the object free space $p_s(t)$ for the individual excitation signals. For the beat signal, a part of 0.25 ms to 0.75 ms of figure 1 left is used for the calculation. It arrives at the receiver positions at 0.89 ms to 1.39 ms. The rest of the beat signal is filled with zeros. So, the beat is used as a quasi-pulse signal. In figure 2 are the two signals depicted. They result in nearly the same pressure field.

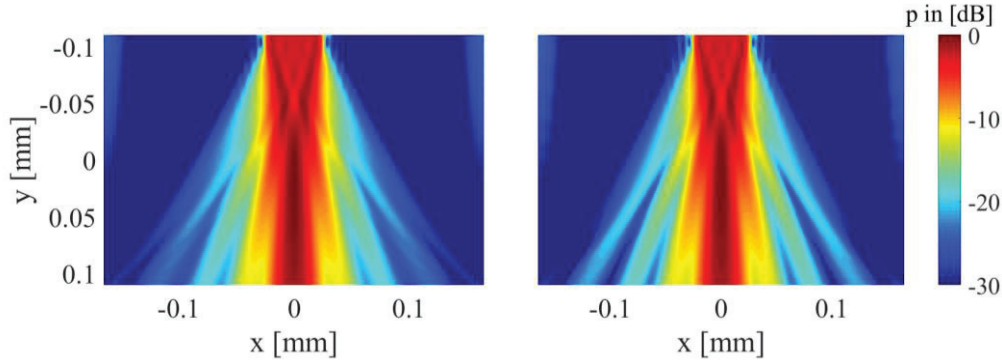


Figure 2 – The backpropagated pressure field of the sine pulse (left) and of the beat signal (right)

2.3 Difference-image

In [3] the authors have shown several threshold methods for the evaluation of difference-images. Here we use a very similar calculation of the threshold hysteresis. For the difference-image method is the object free 2D pressure field of the re-radiation $p_{no,obj}(x, y, \omega)$ and the 2D pressure field with an object $p_{obj}(x, y, \omega)$ been used. Both in dB normalized to the maximum pressure which was recorded at all receivers over the time in the object free space $p_s(t)$. At first a background image must be calculated to make the results better interpretable. The background image B_{xy} is:

$$B_{xy} = \text{med}_{xy,3 \times 3} \left(\left[20 \log_{10} \left(\frac{p_{obj}(x, y, \omega)}{\max(p_s(t))} \right) - 20 \log_{10} \left(\frac{p_{no,obj}(x, y, \omega)}{\max(p_s(t))} \right) \right]^2 \right) \quad (9)$$

A 2D-median-filter $\text{med}_{xy,3 \times 3}$ with a 3×3 neighbourhood is used to smooth the background image. With this image the difference-image D_{xy} is calculated of:

$$D_{xy} = \left| 20 \log_{10} \left(\frac{p_{obj}(x, y, \omega)}{\max(p_s(t))} \right) - B_{xy} \right| \quad (10)$$

In a further step, the difference-image can be processed to a peak border image of the median absolute deviation:

$$MAD = \text{med}_{xy,3 \times 3} (|D_{xy} - \text{med}_{xy,3 \times 3}(D_{xy})|) \quad (11)$$

To get well interpretable pictures in MATLAB the colormap 'grey' is used. For the median absolute deviation the colour axis has its limits from 0 to the minimum of the median absolute deviation which is greater than zero $\min_{xy}(MAD > 0)$. It has been shown empirically that these are good values. For the difference-image the colour axis has his limits from the minimum of the difference-image $\min_{xy}(D_{xy})$ to the maximum $\max_{xy}(D_{xy})$. Only these pixels are displayed which follows the pixel wise calculated threshold R with the upper and lower threshold to get a borderline image of the difference-image with $1.0035 < R \leq 1.005$:

$$R = \sqrt{\frac{\ln(2)}{\ln\left(\frac{1 + 2D_{xy}}{1 + D_{xy}}\right)}} \quad (12)$$

3. Results of the using sine pulse signal

In this section, the results from the sine pulse signal as excitation are discussed. For that, the airborne sound field without and with an object is simulated the sound pressure signals at the receivers

positions are recorded (see section 2.1). Out of these data's the airborne sound field is calculated with the re-radiation method (see section 2.2). Using the proposed difference-image method (see section 2.3) D_{xy} - and MAD -images are used for the object identification. At first the object position, then the size and after that the geometry identification is discussed. In figure 3 are in the first column the difference-images (D_{xy} -images) including the placed object. So, the reader knows where the object is placed. In these images only the pixels are shown which are in the upper threshold (see section 2.3). In the middle column the D_{xy} -images without the object and only the pixels are shown which are in between the upper and lower threshold (see section 2.3). The right column are the peak border images of the median absolute deviation (MAD -image). The images in each row belong together.

The first three rows are for the object position identification in the sound field. In these rows a circular object with a diameter of 20 mm are placed. In the first row are the object centre is at $y= 30$ mm and $x= 0$ mm. That the object is at $x= 0$ mm can be clearly seen out of the symmetry of these three images. The y -position can be determined out of the turbulence line in image c). The re-radiation method can only calculate correct up to the object, because the equation doesn't consider objects in the sound field, so, these turbulences line will be produced. So, in the MAD -image is a turbulence line (this line is once shown in image c) on the right side in red as example). Out of this line the vertical position of the centre of a circular object can be determined to $y= 30$ mm \pm 2 mm. The diameter can be determined from the D_{xy} -image b) of the border's in the middle of the image (red arrow) to $d= 19.5$ mm \pm 1 mm. In the same way the size and position of the object in the second row can be determined to $d= 19.5$ mm \pm 1 mm and $y= 90$ mm \pm 2 mm and $x= 0$ mm. In third row, the object identification is possible of utilizing the MAD -image. Due to the free sound path and that the object is not in the way of the main lobe there are only some peak borders. Some turbulences can be seen on the right but its not possible to identify the position clearly, it's only possible to identify the existence of an object. In the D_{xy} -images g) and h) it is clearer where the object is, because only the sound path from the transducer to the object make big differences and only these can be seen in these images. It can be determined that the object is at $x= 100$ mm \pm 2 mm and that the diameter is $d= 19$ mm \pm 1 mm. The y position is determined to $y= 30$ mm \pm 2 mm.

The fourth and fifth row are for the size determination in comparison to row one. The object in the fourth row has a diameter of $d= 10$ mm and a centre position of $x= 0$ mm and $y= 30$ mm. In the fifth row the object has a diameter of $d= 80$ mm and a centre position of $x= 0$ mm and $y= 30$ mm.

The x -position is clear to determine, because the images are symmetrically so $x= 0$ mm. The y position of the centre can be determined by the turbulence line in the MAD -images l) and o) to $y= 30$ mm \pm 2 mm. Like it is shown in row one in image b) the diameter can be determined from the width of the borders of the D_{xy} -images k) and n) to $d= 9.5$ mm \pm 1 mm in k) and $d= 79.5$ mm \pm 1 mm in n).

The sixth and seventh row are for the geometry identification of the object. In row sixth is a quadratic object with a side length of $a= 20$ mm placed with the centre position $x= 0$ mm and $y= 30$ mm. In the seventh row is an equiangular triangle placed with a side length of 20 mm and a centre position of $x= 0$ mm and $y= 30$ mm.

From the borders of the D_{xy} -image q) can be determined that the object is not circular, it must have vertical borders, because the borders in the image are vertical and not circular like in the images above. From the distance of the vertical borders can one side length determined to $a= 19$ mm \pm 1 mm. The upper end of the quadratic object is at the borders which are positioned on the vertical lines inclining away from the middle to the left and right in image q). The lower end is at the turbulence line in the MAD -image. In contrast to the circular objects is the turbulence line not a marker for the centre of the quadratic object. This is due to the geometric shape and to the re-radiation method. The sound waves path is with a circular object more like a sound lens and with the quadratic object more like a piston transducer. So, the other side length of the quadratic object can be determined to $a= 20$ mm \pm 2 mm. Due to the symmetric behaviour of the images the x position is determined to $x= 0$ mm and the y position can be determined from the side length and the upper or lower edges to $y= 30$ mm \pm 2 mm. The x position of the triangle in the seventh row can be determined due to the symmetric shape of the images to $x= 0$ mm. The lower edge of the triangle is at the turbulence line in the MAD -image and the triangle stands on four peak borders in the D_{xy} -images s) and t). So, the lower edge can be good determined to $y= 40$ mm \pm 0.5 mm. The peak of the triangle is placed between two difference borders and on the left and right of the triangle there are two difference dots which delimit the triangle and barely touch it. Out of this information the triangle can be build.

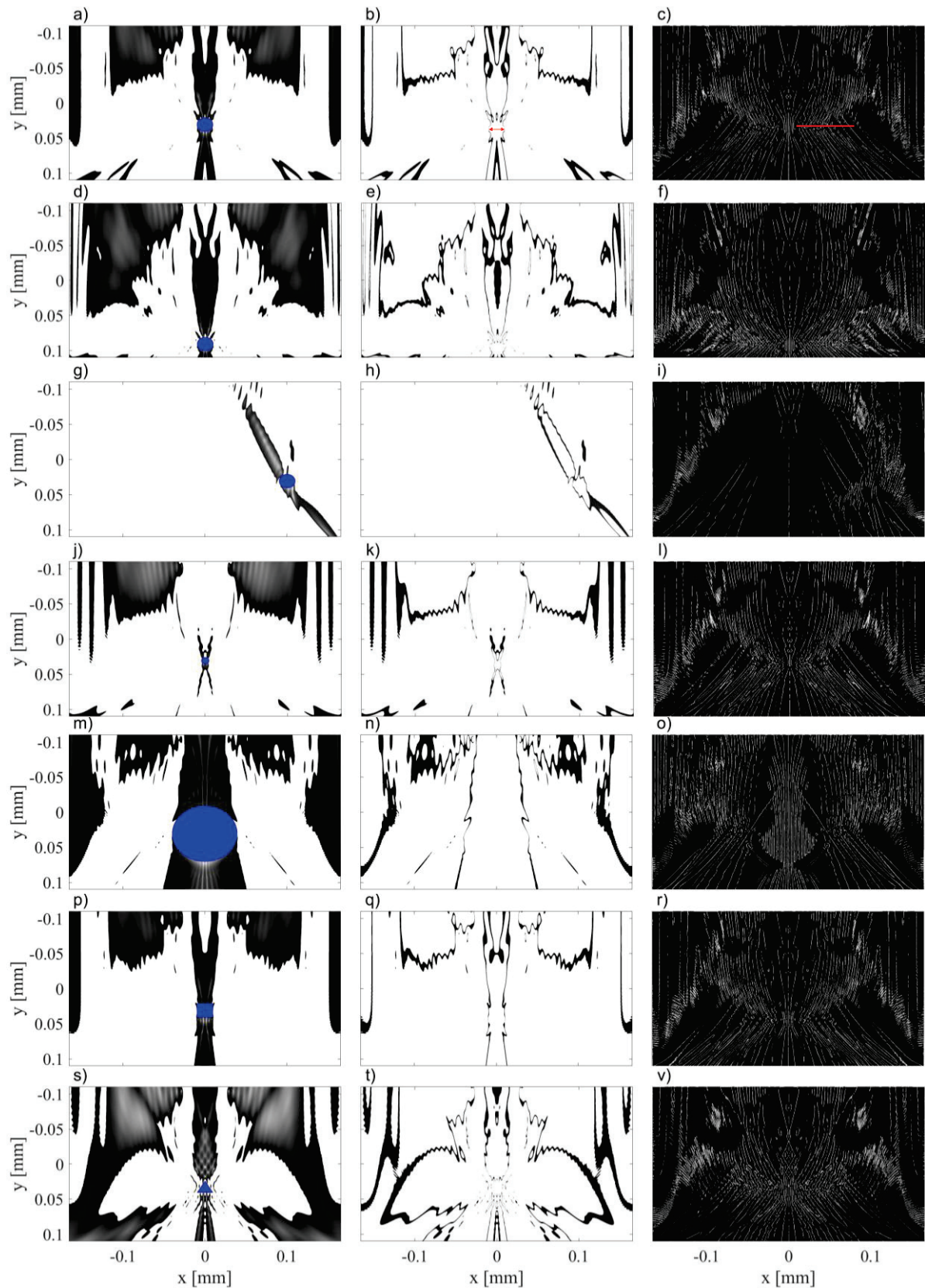


Figure 3 –The left column are D_{xy} -images with the upper threshold with placed PMMA objects a), d) and g) with a circular object and a diameter of 20 mm. j) with a diameter of 10mm, m) with a diameter of 80 mm, p) is quadratic with a side length of 20 mm and s) is an equiangular triangle with the side length of 20 mm. The middle column are D_{xy} -images with the upper and lower threshold. The right column are the MAD -images. The images in a row belong together.

4. Results of the using beat signal

In this section, the results from the beat signal as excitation are discussed. For that, the airborne sound field without and with an object is simulated the sound pressure signals at the receivers positions are recorded (see section 2.1). Out of these data's the airborne sound field is calculated with the re-radiation method (see section 2.2). Using the proposed difference-image method (see section 2.3) D_{xy} - and MAD -images are used for the object identification. In figure 4 the results of the beat signal are depicted. In the first column are the D_{xy} -images with the placed object, so, the reader knows where the object is placed. In these images only these pixels are shown which are in the upper threshold (see section 2.3). In the middle column the D_{xy} -images without the object and only these pixels are shown which are in between upper and lower threshold (see section 2.3). The right column are the peak border images of the median absolute deviation (MAD -image). The images in a row belong together.

In the first row the same circular object like in figure 3 in the first row is placed. It has a diameter of $d= 20$ mm at $x= 0$ mm and $y= 30$ mm. On the first look the images looks nearly equal to the images with utilizing the sine pulse signals, however there are some differences. The position and size of the circular object can be determined like with the sine pulse signal in section 3. In comparison with the first row of figure 3 the sound path of the main lobe doesn't have big differences. The differences are outside of the main lobe, outside of the area where the object is placed. For $y>50$ mm the borders of the D_{xy} -images have changed and there are some new, but there are not important for the determination of the object. On the left and right edge of the D_{xy} -images the borders look more rippled, but this is not an important difference for the object identification. The MAD -image has more turbulences in the peak borders, but the horizontal turbulence line could even good determined.

The second row of figure 4 depict the results for the quadratic object. It's the same quadratic object like in figure 3 row six. It has a side length of $a= 20$ mm and it's placed at $x= 0$ mm and $y= 30$ mm. The object position and geometry identification can be done like in section 3 with the sine pulse signal. The largest difference to the result of the sine pulse signal is, that in the bottom of the D_{xy} -images d) and e) are some border areas. These borders are far away of the place where the object is, so there are not important for the object identification. Like in the images with the circular object, the borders where the object is not, looks more rippled than with the sine pulse signal as excitation signal. These ripples make the peak borders in the MAD -image more turbulence.

In the third row of figure 4 the same equiangular triangle is placed like in figure 3 in the seventh row. It has a side length of 20 mm and a centre position of $x= 0$ mm and $y= 30$ mm. The position and geometric shape can be determined like in section 3, but in these images are more differences than in the images before with the other geometric shaped objects. It determined out of the borders in the D_{xy} -images g) and h) that there is a triangle object. The four border peaks in these images, at the triangle position, can also be determined. The upper peak of the triangle is also placed between two difference borders. On the left and right of the triangle there are no longer two difference dots which delimit the triangle and barely touch it. This makes the reconstruction of the triangle less accurate. Above the triangle in image g) in comparison to figure 3 image s) there are no longer rhombic shaped difference peaks. It's the same in figure 4 i) in comparison to figure 3 v). There are vertical lines now. Just as with the other geometric shaped objects, the borders in the D_{xy} -images g) and h) looks more rippled than with the sine pulse signal.

5. Conclusion

We have shown, with these model-based results, the good applicability of the re-radiation method in conjunction with a difference-image method to identify objects in a 2D sound field. With a sine pulse signal, the position identification and the determination of the geometric shape works well. With the D_{xy} -images, it is possible to determine the position up to an accuracy of 1 mm. The precision of the determination of the geometric shape of the object is clearly possible. The results of the beat signal show nearly equal results to the sine pulse signal. This open the opportunity to use resonant working transducers and to use electronic equipment for harmonic signals, which are not so expensive like for pulse signals, and to use the good characteristics of the pulsed signal. The results must be verified in future experiments but our results provide a new way to object description or identification from the recording of airborne sound fields.

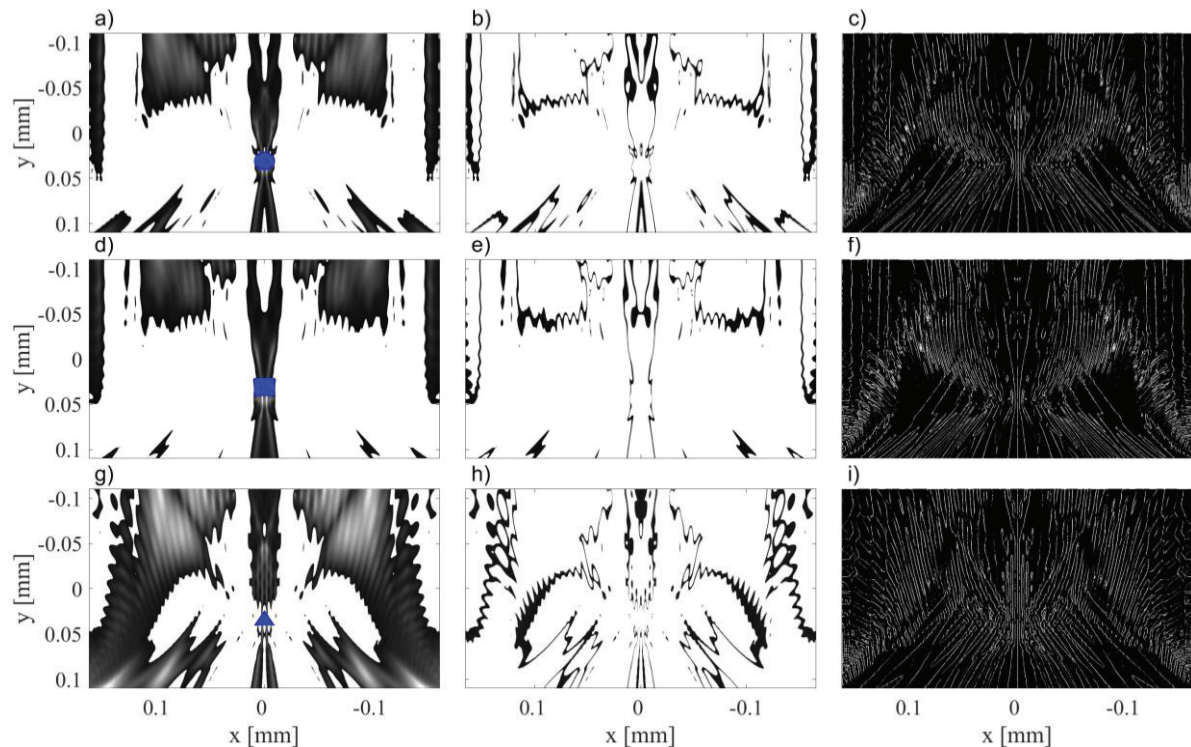


Figure 4 – The left column are D_{xy} -images with the upper threshold with placed PMMA (blue) objects a) with a circular object and a diameter of 20 mm. d) is quadratic with a side length of 20 mm and g) is an equiangular triangle with the side length of 20 mm. The middle column are D_{xy} -images with the upper and lower threshold. The right column are the MAD -images. The images in a row belong together.

REFERENCES

- Sanabria SJ, Marhenke T, Furrer R, Neuenschwander J. Calculation of volumetric sound field of pulsed air-coupled ultrasound transducers based on single-plane measurements. *IEEE transact. on ultrasonic, ferroelectrics, and frequency control*. vol. 65, 2018, p. 72-84
- Tsysar SA, Sapozhnikov OA. Ultrasonic holography of 3D objects. *2009 IEEE int. ultrasonics symp. proc.* 2009. p. 737- 740. ISBN 978-1-4244-4390-1/09
- Rosin PL, Ellis TJ. Image difference threshold strategies and shadow detection. *BMVC 1995*, doi:10.5244/C.9.35
- Knoll AC. Ultrasonic holography techniques for localizing and imaging solid objects. *IEEE transact. on robotics and automation*, vol. 7, 1991 p. 449-467
- Treeby B, Cox B, Jaros J. *k-Wave User Manual*. Manual Version 1.0.1. 2012
- Fathizadeh Z, Aboonajmi M. Nondestructive air-coupled ultrasound measurement in the food industries. *Proc IRNDT 2017*; 26-27 February 2017; Teheran, Iran 2017.
- Fang Y, Lin L, Feng H, Lu Z, Emms GW. Review of the use of air-coupled ultrasonic technologies for nondestructive testing of wood and wood products. *Computers and Electronics in Agriculture*. vol. 137, 2017, p. 79-87
- Marhenke T, Sanabria SJ, Chintada BR, Furrer R, Neuenschwander J, Goksel O. Acoustic field characterization of medical array transducer based on unfocused transmits and single-plane hydrophone measurements. *Sensors*. vol. 19, 2019, 863, doi:10.3390/s19040863
- Marhenke T, Sanabria SJ, Twiefel J, Furrer R, Neuenschwander J, Wallaschek J. Three-dimensional sound field computation and optimization of the delamination detection based on the re-radiation. *ECNDT 2018*; 11-15 June 2018; Gothenburg; Sweden